Research Article

Álvaro Rodríguez Echarri, Joel D. Cox and F. Javier García de Abajo*

Direct generation of entangled photon pairs in nonlinear optical waveguides

https://doi.org/10.1515/nanoph-2021-0736
Received November 27, 2021; accepted January 10, 2022; published online January 21, 2022

Abstract: Entangled photons are pivotal elements in emerging quantum information technologies. While several schemes are available for the production of entangled photons, they typically require the assistance of cumbersome optical elements to couple them to other components involved in logic operations. Here, we introduce a scheme by which entangled photon pairs are directly generated as guided mode states in optical waveguides. The scheme relies on the intrinsic nonlinearity of the waveguide material, circumventing the use of bulky optical components and their associated phase-matching constraints. Specifically, we consider an optical waveguide under normal illumination, so that photon down-conversion can take place to excite waveguide states with opposite momentum in a spectral region populated by only two accessible modes. By additionally configuring the external illumination to interfere different incident directions, we can produce maximally entangled photon-pair states, directly generated as waveguide modes with conversion efficiencies that are competitive with respect to existing macroscopic schemes. These results should find application in the design of more efficient and compact quantum optics devices.

Keywords: entangled guided modes; nonlinear optics; optical down-conversion; quantum optics.

***Corresponding author: F. Javier García de Abajo**, ICFO-Institut de Ciencies Fotoniques, The Barcelona Institute of Science and Technology, 08 860 Castelldefels, Barcelona, Spain; and ICREA-Institució Catalana de Recerca i Estudis Avançats, Passeig Lluís Companys 23, 08 010 Barcelona, Spain,
E-mail: javier.garciadeabajo@nanophotonics.es. https://orcid.org/0000-0002-4970-4565
Álvaro Rodríguez Echarri, ICFO-Institut de Ciencies Fotoniques, The Barcelona Institute of Science and Technology, 08 860 Castelldefels, Barcelona, Spain, E-mail: arepb15@gmail.com. https://orcid.org/0000-0003-4634-985X
Joel D. Cox, Center for Nano Optics, University of Southern Denmark, Campusvej 55, DK-5230 Odense M, Denmark; and Danish Institute for Advanced Study, University of Southern Denmark, Campusvej 55, DK-5230 Odense M, Denmark, E-mail: cox@mci.sdu.dk. https://orcid.org/0000-0002-5954-6038

1 Introduction

As quantum information processing is reaching a mature state, different platforms that materialize quantum entanglement are being intensely explored [1–4]. Among them, the generation of entangled photon pairs via nonlinear light–matter interactions is highly appealing for practical implementation, where photons – being capable of traversing enormous distances at the ultimate speed while interacting weakly with their environment – are ideal carriers of information [5, 6]. In this context, the intrinsically weak interaction of light with matter is both a blessing and a curse, in that propagating photons are less sensitive to decoherence, but are difficult to manipulate because they cannot be easily brought to interact [7]. Efficient harvesting of generated entangled photon pairs in optical device architectures presents further technological challenges that impede development of all-optical quantum information networks.

Quantum entanglement has traditionally been encoded in the polarization (or spin angular momentum) state of photons funneled into the weakly guided modes supported by optical fibers [8, 9]. Alternatively, the orbital angular momentum (OAM) state of light constitutes an infinite basis set in which photon entanglement is accessed by twisting the light wavefront [10–12]. Recently, optical metasurfaces capable of generating light in arbitrary spin and OAM states have been employed to produce well-collimated streams of entangled photons [13, 14].

Entangled photon pairs are typically generated via spontaneous parametric down-conversion (SPDC) [15, 16], a second-order nonlinear optical process that is tantamount to time-reversed sum-frequency (SF) generation [17–19], and which conserves both spin and OAM. However, the generation and manipulation of entangled light is hindered not only by the low nonlinear response of conventional materials, but also by the need to collect and direct the entangled photon pairs – produced upon phase-matching in bulk nonlinear crystals – into scalable optical components that enable quantum logic operations. Theoretical explorations of SPDC by waveguided photons have revealed its feasibility in the presence of

material dispersion and loss [20–22], while experimental efforts to develop on-chip sources of entangled photons include demonstrations of SPDC in periodically poled $LiNbO_3$ waveguides [23, 24] and in a microring resonator [25, 26], as well as path-entanglement photons based on coupled waveguides in on-chip direct-illumination schemes [27, 28]. Additionally, the SPDC process has been recently proposed to conserve the in-plane momentum in graphene ribbons containing an electrostatically induced p–n junction where entangled plasmonic modes are generated [29].

In this work, we propose an alternative strategy to excite entangled photon pairs directly into a low-loss optical waveguide simply by illuminating it from free space, and explore the feasibility of this approach through rigorous theoretical analysis. Our method relies on the intrinsic second-order optical nonlinearity of the waveguide to down-convert a normally impinging optical field directly into two guided modes, where energy and momentum conservation restricts the possible modes that can be accessed by a particular incident field. To quantitatively analyze the down-conversion scheme, we consider the reverse process, in which two counter-propagating waveguide modes up-convert into a free-space photon mode. By invoking the reciprocity theorem [30], our analysis effectively describes the fidelity of our proposed SPDC scheme, which can be readily explored in an experimental setting using conventional optical components, and thus provides a widely accessible source of entangled photon pairs directly generated in an optical waveguide. Although different counter-propagating illumination schemes involving optical waveguides have been proposed [31–35], we emphasize that here entanglement does not rely on phase-matching, and takes place directly within the waveguide modes.

2 Results and discussion

We consider the configuration shown in Figure 1(a), consisting of a freestanding cylindrical waveguide of radius a under normal illumination. For simplicity, we assume isotropic, homogeneous materials, although our calculations can be readily extended to anisotropic media and more complex geometries, such as a noncircular waveguide on a substrate. As we elaborate in Methods, the cylindrical waveguide geometry admits analytical expressions that characterize the electromagnetic field profiles of its guided modes and their dispersion. The latter is presented in Figure 1(b), and represents a dispersion relation typical for high-index dielectric waveguides, including those with a rectangular cross-section, as we show in the Supplementary Information (SI). The second-order nonlinearity of the waveguide material facilitates SPDC

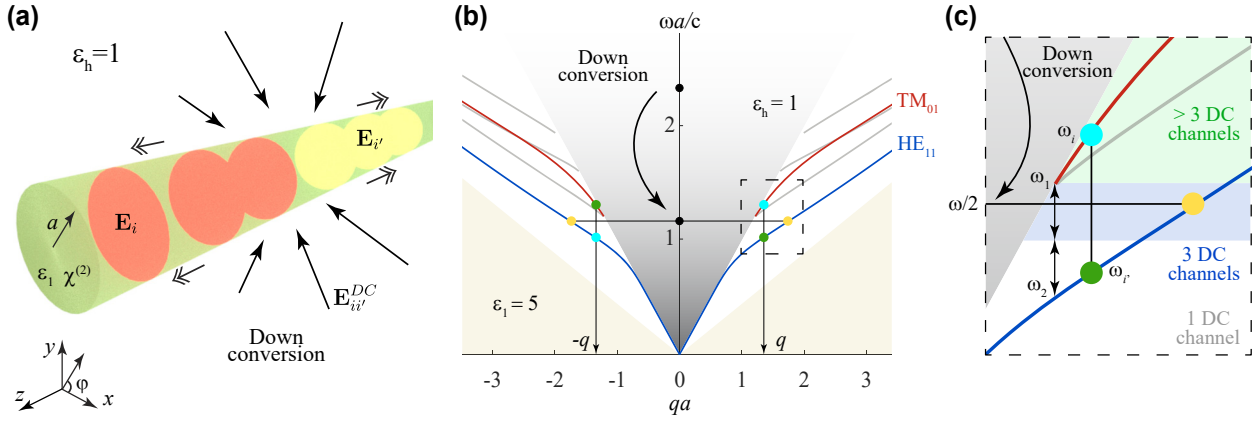

Figure 1: Generation of waveguided entangled photon pairs by down-conversion in an optical waveguide.
(a) Illustration of a cylindrical waveguide (radius a, material permittivity ϵ_1, and host permittivity ϵ_h) subject to normal illumination. Each incident photon can be down-converted via the second-order nonlinear response of the waveguide material (susceptibility $\chi^{(2)}$) to produce two waveguided photons within modes i and i' characterized by electric fields $\mathbf{E}_i$ and $\mathbf{E}_{i'}$, frequencies ω_i and $\omega_{i'}$, and wave vectors q_i and $q_{i'}$ satisfying $q_i + q_{i'} = 0$. (b) Dispersion diagram of waveguide modes (normalized frequency $\omega a/c$ as a function of normalized wave vector qa) for $\epsilon_1 = 5$ and $\epsilon_h = 1$. The light cones in the waveguide and host materials (white and gray areas, respectively) limit the existence of guided modes. We highlight the two lowest-order modes that possess nonzero longitudinal field components (HE_{11} and TM_{01}, see labels) and enable down-conversion with a small number of photon-pair emission channels: one symmetric (yellow circles) and two asymmetric (blue and green circles) channels. (c) Detail of photon-pair emission channels, showing the threshold frequency of the TM_{01} mode ω_1, the frequency ω_2 of the HE_{11} mode with the same wave vector, and the number of down-conversion channels available depending on the incident photon frequency ω (1, 3, and >3 in white, blue, and green areas). Each channel has $\pm q$ and $\pm m$ degeneracies.

into states lying within different bands, so that an incident photon is converted into two guided photons, with wave vectors of opposite sign (q and $-q$) that conserve momentum along the direction of translational invariance, as sketched in Figure 1(b) and discussed below.

Without entering into the details of how to quantify entanglement for more complex states [36], we aim at producing maximally entangled photon pairs moving in opposite directions along the waveguide (left L with wave vector $-q$, and right R with wave vector q) that correspond to Bell quantum states of the form

$$|\psi\rangle = |L_i R_{i'}\rangle + |L_{i'} R_i\rangle, \tag{1}$$

where i and i' denote different photon quantum numbers, such as the azimuthal number m, the mode polarization, and the frequency. Before exploring these possibilities, we provide a rigorous theory to calculate the SPDC efficiency associated with different output channels in the waveguide.

2.1 Down-conversion efficiency in cylindrical waveguides

To quantify the SPDC efficiency, we compute the probability of the inverse process: SF generation produced by two counter-propagating guided photons of frequencies ω_i and $\omega_{i'}$ which combine to generate a photon frequency $\omega_{ii'} = \omega_i + \omega_{i'}$ that is normally emitted from the waveguide. In virtue of reciprocity, the per-photon probabilities for the two processes (SPDC and SF generation) are identical. In practice, we calculate the efficiency by considering two photons within counter-propagating guided modes i and i', prepared as long pulses of length L and space/time-dependent electric fields $\mathbf{E}_i(\mathbf{r}, t)$ and $\mathbf{E}_{i'}(\mathbf{r}, t)$ (Figure 1(a)) that comprise frequency components that are tightly packed around ω_i and $\omega_{i'}$. Through the SF second-order susceptibility tensor $\chi^{(2)}$, a polarization density $\mathbf{P}_{ii'}(\mathbf{R})$ is produced within a narrow frequency range around $\omega_{ii'}$. More precisely,

$$\tilde{P}_{ii',a}(\mathbf{R}) = \sum_{bc} \frac{\chi^{(2)}_{abc}(\mathbf{R})}{|\bar{\chi}^{(2)}|} E_{i,b}(\mathbf{R}) E_{i',c}(\mathbf{R}), \tag{2}$$

where the indices $\{a, b, c\}$ run over Cartesian components, $\mathbf{E}_i(\mathbf{R})$ gives the profile of mode i in the transverse plane $\mathbf{R} = (x, y)$, and we normalize the susceptibility to the quantity

$$|\bar{\chi}^{(2)}| \equiv \sum_{abc} |\chi^{(2)}_{abc}|. \tag{3}$$

For simplicity, we consider the wave vectors of the two modes to satisfy the condition $q_i + q_{i'} = 0$, so that the SF photons are emitted with zero wave vector component parallel to the waveguide (i.e., along normal directions). The SF polarization density generates a field that we compute at long distances from the waveguide using the electromagnetic Green tensor of the system $\mathcal{G}(\mathbf{r}, \mathbf{r}', \omega)$ [22], from which we calculate the far-field Poynting vector, whose radial component is in turn integrated over time and directions of emission to produce the emitted energy. We then divide this energy by $\hbar\omega_{ii'}$ to obtain the number of emitted photons $N_{ii'}$. Likewise, we calculate the Poynting vector associated with each of the pulses and integrate the component parallel to the waveguide over time and transverse spatial directions to yield the number of photons incident in each pulse, N_i and $N_{i'}$. Finally, the ratio of the emitted number of photons to the number of photons in each pulse is interpreted as the probability $\eta_{ii'} = N_{ii'}/N_i N_{i'}$ that two colliding quanta combine into one emitted SF quantum (again, identical with the probability that an externally incident photon produces a pair of counter-propagating photons within modes i and i'). In the long L limit, the incident pulses become monochromatic and $\eta_{ii'}$ turns out to be independent of L. For convenience, we decompose the up-conversion efficienty into contributions associated with emission along different azimuthal angles φ (see coordinate system in Figure 1(a)) as

$$\eta_{ii'} = \int_0^{2\pi} \mathrm{d}\varphi \eta_{ii'}(\varphi). \tag{4}$$

After a lengthy calculation (see a detailed self-contained derivation in Methods), we obtain the following result for the angle-resolved efficiency:

$$\eta_{ii'}(\varphi) = \frac{4\pi^2\hbar c}{a^4} |\bar{\chi}^{(2)}|^2 \frac{w_i w_{i'}}{(w_i + w_{i'})^2} \frac{|\beta_i \beta_{i'}|}{|\beta_i| + |\beta_{i'}|} \frac{I_{ii'}(\varphi)}{I_i I_{i'}}, \tag{5a}$$

$$I_i = \frac{1}{a^2} \int \mathrm{d}^2\mathbf{R}\, \mathrm{Re}\left\{ E_{i,x}(\mathbf{R}) H^*_{i,y}(\mathbf{R}) - E_{i,y}(\mathbf{R}) H^*_{i,x}(\mathbf{R}) \right\}, \tag{5b}$$

$$I_{ii'}(\varphi) = \left| \int_{R'<a} \mathrm{d}^2\mathbf{R}'\, \mathbf{g}\left(\varphi - \varphi', R', \omega_{ii'}\right) \cdot \tilde{\mathbf{P}}_{ii'}(\mathbf{R}') \right|^2, \tag{5c}$$

where $w_i = \omega_i a/c$, $\beta_i = v_i/c$, $v_i = \partial\omega_i/\partial q_i$ is the group velocity in mode i, $\mathbf{H}$ is the magnetic field, and $\mathbf{g}(\varphi - \varphi', R', \omega)$ is the amplitude of the electromagnetic Green tensor in the far-field limit defined through $\mathcal{G}(\mathbf{r}, \mathbf{r}', \omega) \to (\mathrm{e}^{\mathrm{i}\sqrt{\epsilon_\mathrm{h}}\omega R/c}/R)\, \mathbf{g}(\varphi - \varphi', R', \omega)$ for

normal emission (see Eq. (34) below for an explicit expression). Here, I_i and $I_{ii'}$ are proportional to the number of incident photons in waveguide mode i and emitted outside the waveguide, respectively. Incidentally, these coefficients are normalized in such a way that they are independent of the waveguide radius a, so the efficiency $\eta_{ii'}$ only depends on a through an overall factor $1/a^4$ for a fixed value of $\omega_i a/c$. In brief, $\eta_{ii'}$ represents the ratio of SF photons produced per two incident photons (one in each waveguide mode), that is, the SF matrix element for $\omega_i + \omega_{i'} \to \omega_{ii'}$, which must be equal to the SPDC matrix element corresponding to $\omega_{ii'} \to \omega_i + \omega_{i'}$. The latter affects each incident photon separately, so it can be interpreted as the fraction of incident photons that undergo SPDC, and we thus equate it to the fraction of down-converted power.

For the cylindrical waveguides under consideration, we can multiplex the mode labels as $i = \{q_i, m_i, l_i, \sigma_i\}$, where q_i is the wave vector, m_i is the azimuthal angular momentum number, l_i refers to different radial resonances, and σ_i runs over polarization states (i.e., TE_{0l_i} and TM_{0l_i} for $m_i = 0$, and hybrid modes $\mathrm{HE}_{m_i l_i}$ and $\mathrm{EH}_{m_i l_i}$ for $m_i \neq 0$, see Section 4.1.1). Given the symmetry of the waveguide, the radial and azimuthal components of the transverse field associated with each mode only depend on radial distance R, apart from an overall phase factor $\mathrm{e}^{\mathrm{i}m_i\varphi}$. For simplicity, we consider a second-order response tensor $\chi^{(2)}$ that also preserves the cylindrical symmetry, so that the angular integral in Eq. (5c) leads to angular momentum conservation ($m_{ii'} = m_i + m_{i'}$ for the emitted photons). In particular, we assume a nonlinear tensor dominated by the $\chi^{(2)}_{zzz}$ component (e.g., a $LiNbO_3$ waveguide with the z axis aligned along the waveguide), which implies that the TE modes and the TE component of the hybrid modes do not couple to the incident field through $\chi^{(2)}$. In fact, as we show in the Supplementary Information, the mode profiles and dispersion properties of cylindrical waveguides are remarkably similar to their counterparts with rectangular geometries, such as those more commonly employed in the construction of waveguides from highly nonlinear crystals in which a single component of the $\chi^{(2)}$ tensor dominates [37, 38].

2.2 Availability and efficiency of different down-conversion channels

We are now equipped to discuss the generation of entangled photon pairs through SPDC in our waveguide. Assuming the above conditions, the lowest-frequency modes that possess a nonzero z component of the electric field, and can consequently couple to normally impinging external light, are HE_{11} and TM_{01} (see Figure 1(b)). We identify two relevant frequencies in this region (see Figure 1(c)): the threshold of the TM_{01} mode at ω_1 (satisfying $\omega_1 a/c = 2.4048/\sqrt{\epsilon_1 - \epsilon_\mathrm{h}}$, see Section 4.1), and the frequency ω_2 of mode HE_{11} with the same wave vector. Upon inspection, we find that for an incident light frequency $\omega < \omega_1 + \omega_2$, the only SPDC channel available corresponds to the generation of two HE_{11} modes of frequency $\omega/2$ and opposite wave vectors. This situation already allows us to produce entangled photon pairs of the form given in Eq. (1), where i and i' now refer to the azimuthal numbers $m_i, m_{i'} \in \{-1, 1\}$ for each of the emitted photons. In particular, if the waveguide is symmetrically illuminated along different azimuthal directions (see Section 2.3 below), it is possible to select only the $m = 0$ component from the external light, so that conservation of azimuthal angular momentum leads to the condition $m_i + m_{i'} = 0$, and therefore, the emitted photon pair forms an entangled state $|L_{-1}R_1\rangle + |L_1R_{-1}\rangle$, where the subindices indicate the values of m_i and $m_{i'}$ for the L and R emission directions, all of them sharing the same frequency $\omega/2$ and polarizations $\mathrm{HE}_{\pm1,1}$, so we refer to this channel as $\mathrm{HE}_{11} + \mathrm{HE}_{11}$.

Another interesting range of incidence frequencies is $\omega_1 + \omega_2 < \omega < 2\omega_1$ (blue area in Figure 1(c)), where the $\mathrm{HE}_{11} + \mathrm{HE}_{11}$ channel is now supplemented by two additional possibilities in which the two generated photons have different frequencies (with the sum satisfying $\omega = \omega_i + \omega_{i'}$) and lie in different bands (HE_{11} or TM_{01}). This is indicated by the two pairs of color-matched blue and green dots in Figure 1(b) and (c), where the condition of opposite wave vectors is obviously satisfied. Again, it is possible to select a specific SPDC channel by illuminating with a fixed m number (see below), and in particular, by setting $m = m_i + m_{i'} = 1$, the $\mathrm{HE}_{11} + \mathrm{HE}_{11}$ channel is eliminated (because the overall azimuthal number obtained by combining two $\mathrm{HE}_{\pm11}$ modes is 0 or ±2), so that we obtain again a maximally entangled state of the form given in Eq. (1) with i and i' now referring to TM_{01} and HE_{11} (i.e., $|L_\mathrm{TM}R_\mathrm{HE}\rangle + |L_\mathrm{HE}R_\mathrm{TM}\rangle$, with azimuthal numbers m_i and $m_{i'}$ taking the values 0 and 1 in the TM and HE components, respectively).

The formalism presented in Section 2.1 allows us to calculate the SPDC efficiency for the production of specific photon pair-states, using external illumination prepared with an azimuthal number $m = m_i + m_{i'}$ and a polarization state determined by the time reversal of the SF generation state considered in the derivation of these results. Under the assumed conditions of incidence along transverse directions, and considering a zzz-dominant component in the second-order susceptibility tensor, the profile of the applied light amplitude as a function of azimuthal angle φ is therefore taken to be $\mathrm{e}^{\mathrm{i}m\varphi}$, with the field oriented parallel

to the waveguide direction. These conditions can be met by combining several incident light beams, as we discuss below. The efficiencies calculated for different SPDC channels in this scheme are shown in Figure 2, normalized to $(\hbar c/a^4)|\bar{\chi}^{(2)}|^2$ in order to present universal, dimensionless results as a function of the scaled incident light frequency $\omega a/c$. For an $\epsilon_1 = 5$ waveguide in air (Figure 2(a)), we find efficiencies that generally grow with the order of the waveguide modes, exhibiting resonances as a function of the incident frequency $\omega = \omega_i + \omega_{i'}$. These resonances are inherited from the two-dimensional transmission coefficients (see Section 4.1) and can be understood as coupling of the incident light to leaky cavity modes at the incident light frequency. We indicate in white the area in which there is only one decay channel ($HE_{11} + HE_{11}$, see above), whereas the area with three decay channels (two additional ones corresponding to $TM_{01} + HE_{11}$ and $HE_{11} + TM_{01}$) is highlighted in blue. The green region at higher frequencies contains an increasing number of channels, which could be also exploited to generate more complex entangled mixtures, involving multiple output states in each direction (L and R) and higher-order modes.

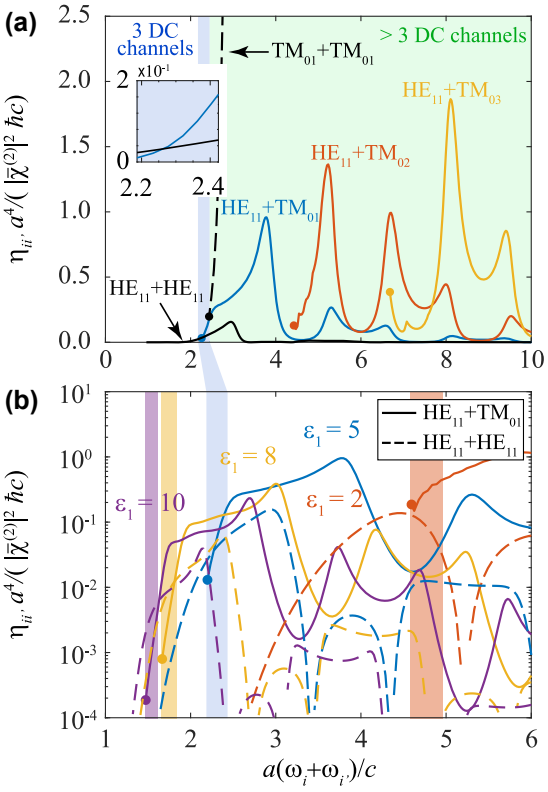

Figure 2: Down-conversion efficiency for different output channels. (a) Normalized SPDC efficiency for a waveguide with $\epsilon_1 = 5$ and $\epsilon_h = 1$ as a function of incident light frequency $\omega = \omega_i + \omega_{i'}$. Different output channels i+ i' are indicated by labels, while the regions highlighted in white, blue, and green indicate 1, 3, and >3 available channels (each of them degenerate in the sign of both the wave vectors and the azimuthal numbers). (b) Efficiencies corresponding to the three lowest channels (one in $HE_{11} + HE_{11}$ and two in $HE_{11} + TM_{01}$) for different values of the waveguide permittivity ϵ_1 (see color-coded labels). Colored areas highlight the respective regions in which three channels exist, while the frequency threshold for each of the down-conversion channels is indicated by colored circles.

The spectral evolution of the efficiencies is roughly maintained when varying the waveguide permittivity ϵ_1 (Figure 2(b)), but we observe a general increase in $\eta_{ii'}$ with increasing ϵ_1 in the region of interest, as well as a spectral shift of the region with three output channels (highlighted in shading colors and evolving toward lower frequencies as we increase the permittivity, in agreement with the single-mode-fiber cutoff condition). Interestingly, we find a crossover in the efficiency of $HE_{11} + HE_{11}$ relative to that of $HE_{11} + TM_{01}$: the former dominates over the latter within the three-channel region at high ϵ_1, whereas the opposite behavior is found at lower permittivities.

Quantitatively, our results indicate that the current scheme is feasible for producing a reasonable rate of entangled photon pairs, taking into account that they are already prepared within waveguide modes [31, 33]. In particular, for values of $|\bar{\chi}^{(2)}| \sim 10^{-10}$ m V^{-1} found in good nonlinear materials such as $LiNbO_3$ [17, 39] and a waveguide radius ~ 100 nm, the scaling factor in Figure 2 is $(\hbar c/a^4)|\bar{\chi}^{(2)}|^2 \sim 10^{-10}$ upon conversion of the arguments to the Gaussian-GCS unit system adopted here, which yields a power fraction of 10^{-11} for SPDC when it is multiplied by a scaled efficiency of ~ 0.1 (Figure 2). Considering photon energies ~ 1 eV and an incident light power ~ 1 mW, the estimated power fraction amounts to a generation rate of $\sim 10^5$ entangled photon pairs per second. As an additional possibility, the efficiency could be increased by incorporating resonant elements to amplify the external light in the region surrounding the waveguide, such as planar Fabry–Perot resonators, which is a natural option for waveguides fabricated on a substrate [34, 37]. Alternatively, the SPDC efficiency can be improved by physically or chemically doping the waveguide with active centers to enhance its intrinsic nonlinear response, or by incorporating different materials in lithographically patterned waveguide geometries.

2.3 Selection of down-conversion channels through illumination interference

A p-polarized electromagnetic plane wave of amplitude E_0 incident through the host medium with a wave vector $\mathbf{k}_h \perp \hat{\mathbf{z}}$ normal to the waveguide (Figure 3(a)) contributes with a

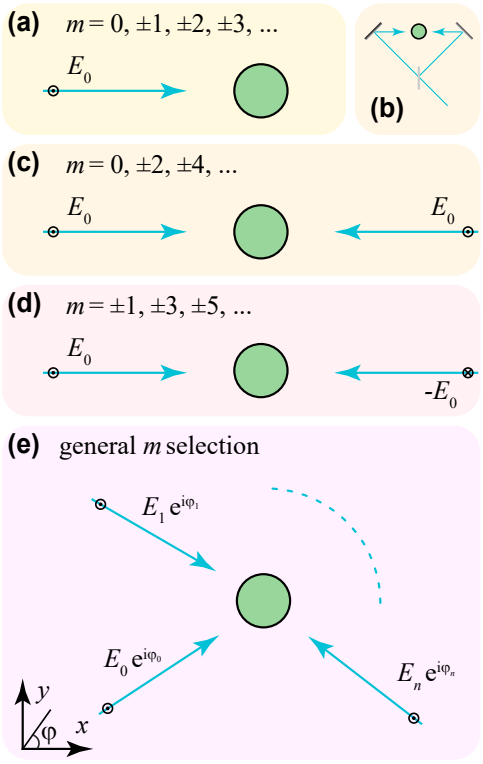

Figure 3: Mode selection through light interference. A single incident light plane wave (a) contains all possible values of the azimuthal number m in the external field, and can thus excite all available SPDC channels for the chosen input frequency. We can combine illumination from different directions through beam splitters and mirrors, as indicated in (b) for two-plane-wave irradiation, leading to a selection of the m values from the external light. Examples of selection by irradiation with two in-phase and out-of-phase counter-propagating plane waves are shown in (c) and (d). More stringent selection of m is possible by combining multiple plane waves of amplitudes E_j along different azimuthal directions φ_j, with $j = 0, \ldots, n$.

broad range of azimuthal numbers $m = m_i + m_{i'}$ according to the decomposition

$$E_0\,\hat{\mathbf{z}}\,e^{i\mathbf{k}_h\cdot\mathbf{R}} = \sum_m i^m E_0 e^{-im\varphi_{\mathbf{k}_h}} \mathbf{E}^J_{h,0mp}(\mathbf{R}) \qquad (6)$$

in terms of cylindrical waves $\mathbf{E}^J_{h,0mp}$ (see Supplementary Information). This situation leads to entangled states that combine more than two polarizations for each of the two waveguiding directions (L and R). For example, in the single $HE_{11} + HE_{11}$ channel region (at incident light frequency $\omega < \omega_1 + \omega_2$), we can have all combinations of $m_i = \pm1$ and $m_{i'} = \pm1$, thus reducing the degree of entanglement. One way to address this issue is to combine illumination from different azimuthal directions (e.g., in an interferometric setup involving beamsplitters and mirrors, as illustrated in Figure 3(b)). In particular, when illuminating with two in-phase counter-propagating waves (Figure 3(c)), only even values of m survive, whereas only odd m's are selected if the waves have a π relative phase difference (Figure 3(d)). In general, we can consider an arbitrary number of plane waves (Figure 3(e)), so that the total field acting on the waveguide has the same form as in Eq. (6), but with $E_0 e^{-im\varphi_{\mathbf{k}_h}}$ substituted by $\sum_j E_j e^{-im\varphi_j}$, where the sum runs over plane waves j of amplitude E_j directed along azimuthal directions φ_j.

In the one-channel regime ($HE_{11} + HE_{11}$ output), we can generate the maximally entangled state $|L_{-1}R_1\rangle + |L_1R_{-1}\rangle$ by selecting an incident $m = 0$ component and eliminating $m = \pm2$ contributions, as other values of m do not couple to the output modes that are available in that region. This selection requires a minimum of three external plane waves (e.g., with equal amplitudes and azimuthal angles of 0 and $\pm\pi/3$). Likewise, a more stringent selection of m contributions is possible by resorting to more incident plane waves, therefore opening a vast range of possible entangled photon pairs prepared in higher-order modes. In particular, a simple discrete-transform analysis leads to the conclusion that we can select a specific $m = m_0$ component while canceling out those of all other m's in the $|m| \leq N$ range by combining $2N + 1$ incident waves along azimuthal directions $\varphi_j = 2\pi j/(2N + 1)$ with amplitudes $E_j = E_0 e^{im_0\varphi_j}$ for $0 \leq j \leq 2N$. For example, in the three-channel region of Figure 2, applying this procedure with $N = 2$, five plane waves can be used to select $m = 1$ (or $m = -1$) while discarding the undesired $m = 0, \pm2$ and $m = -1$ (or $m = 1$) contributions to obtain a maximally entangled state $|L_{TM}R_{HE}\rangle + |L_{HE}R_{TM}\rangle$ that combines the TM_{01} and HE_{11} (or HE_{-11}) modes.

3 Concluding remarks

We propose a straightforward approach to generate entangled photon pairs directly into low-loss dielectric waveguides based on down-conversion of normally impinging light and introduce a theoretical formalism relying on the reciprocity theorem to quantify the efficiency of the process. Our formalism leads to a universal overall scaling of the efficiency η with the second-order nonlinear susceptibility $\chi^{(2)}$ and waveguide radius a as $\eta \propto |\bar{\chi}^{(2)}|^2/a^4$, which is further factored by an involved interplay among material parameters. For a moderate incident light power of 1 mW and an efficient nonlinear material such as $LiNbO_3$, our theory predicts a production rate of $\sim 10^5$ entangled photon pairs per second. The theoretical prescription here presented for cylindrical geometries can be readily

extended to other waveguide configurations, which impose different symmetries. In particular, preferential elements of the nonlinear susceptibility tensor may be more easily accessed in alternative morphologies depending on the material symmetry (e.g., in rectangular waveguides, which are shown in the Supplementary Information to present remarkably similar modal characteristics as their cylindrical counterparts). Integration of the waveguide on a substrate opens additional possibilities to resonantly amplify the external light (e.g., through Fabry–Perot resonators), including exposure to evanescent fields (along the transverse directions) rather than propagating light. Crucially, the investigated strategy to generate counter-propagating photons necessitates only conventional optical elements, while the theory can be directly applied to predict the efficiency of the down-conversion process. Moreover, we suggest interferometric schemes to select the symmetry of the generated photon modes, thus reducing the number of accessible SPDC channels and increasing the resulting degree of entanglement. Frequency post-selection of the generated waveguided photons can also be used to discard undesired channels and enhance entanglement. An implementation of these ideas should enable the generation of down-converted photon pairs with a high degree of entanglement involving on-demand combinations of high-order symmetries. We thus envision that these findings can stimulate experimental ventures in quantum optics to entangle light with a predictable degree of fidelity and help alleviate practical issues related to the coupling of quantum light sources to optical components required in emerging quantum information technologies.

4 Methods

In this section, we provide a detailed, self-contained derivation of the formalism and equations used in the main text. More precisely, we provide the following elements: a description of guided modes in a cylindrical dielectric wire, along with explicit expressions for their associated electromagnetic fields; a discussion of waveguided pulses; a study of the field produced by line dipoles situated inside the waveguide; a calculation of the SF energy that is emitted into the far field through the second-order nonlinearity of the waveguide material in response to two counter-propagating guided pulses; and a derivation of the SF conversion efficiency, which we argue to be equal to the SPDC efficiency in virtue of reciprocity. We consider guided modes with opposite wave vectors (Figure 1(a)), which couple to external light propagating along directions perpendicular to the waveguide.

4.1 Electromagnetic waves in a cylindrical waveguide

To describe electromagnetic waves in a cylindrical geometry, we first decompose the electric field into cylindrical waves following the prescription of Ref. [40]. More specifically, adopting a cylindrical coordinate system $\mathbf{r} = (R, \varphi, z)$, we consider a homogeneous, isotropic dielectric medium (labeled j) free of external charges and currents that is characterized by a permittivity ϵ_j (setting the magnetic permeability to $\mu = 1$) and express the electric field in cylindrical waves indexed by their azimuthal number m, wave vector q along $\hat{\mathbf{z}}$, and polarization $\sigma \in \{s, p\}$ according to

$$\mathbf{E}^J_{j,qms}(\mathbf{r}) = \left[\frac{\mathrm{i}m}{Q_j R} J_m(Q_j R)\hat{\mathbf{R}} - J'_m(Q_j R)\hat{\boldsymbol{\varphi}}\right] \mathrm{e}^{\mathrm{i}m\varphi}\mathrm{e}^{\mathrm{i}qz}, \tag{7a}$$

$$\mathbf{E}^J_{j,qmp}(\mathbf{r}) = \frac{q}{k_j}\left[\mathrm{i}J'_m(Q_j R)\hat{\mathbf{R}} - \frac{m}{Q_j R}J_m(Q_j R)\hat{\boldsymbol{\varphi}} + \frac{Q_j}{q}J_m(Q_j R)\hat{\mathbf{z}}\right] \mathrm{e}^{\mathrm{i}m\varphi}\mathrm{e}^{\mathrm{i}qz}, \tag{7b}$$

where we define $k_j = \sqrt{\epsilon_j}\omega/c$ and $Q_j = \sqrt{k_j^2 - q^2 + \mathrm{i}0^+}$ (with the square root yielding a positive real part), while the primes on the Bessel functions denote differentiation with respect to the argument. From the orthogonality of the Bessel functions $\int_0^\infty x\mathrm{d}x J_m(x)J_m(ax) = \delta(a-1)$, it is easy to show that these fields satisfy the orthonormality relation $\int \mathrm{d}^2\mathbf{R}\, \mathbf{E}^J_{j,qm\sigma} \cdot \left(\mathbf{E}^J_{j,q'm'\sigma'}\right)^* = 2\pi\delta_{mm'}\delta_{\sigma\sigma'}\delta(q-q')/q$, while the field of modes with different polarizations are related as

$$\mathbf{E}^J_{j,qm\sigma} = \frac{1}{k_j}\nabla \times \mathbf{E}^J_{j,qm\sigma'}, \quad \sigma \neq \sigma'. \tag{8}$$

We now discuss a cylindrical wave emanating from the interior of a cylindrical waveguide of radius a that is infinitely extended in the z direction, comprised of a dielectric material of permittivity ϵ_1 (medium $j = 1$), and embedded in a host medium $j = \mathrm{h}$ (permittivity ϵ_h). Using the notation introduced above, the electric field is expressed as

$$\mathbf{E} = \begin{cases} \mathbf{E}^H_{1,qm\sigma} + r_{m,s\sigma}\mathbf{E}^J_{1,qms} + r_{m,p\sigma}\mathbf{E}^J_{1,qmp}, & R < a, \\ t_{m,s\sigma}\mathbf{E}^H_{\mathrm{h},qms} + t_{m,p\sigma}\mathbf{E}^H_{\mathrm{h},qmp}, & R \geq a, \end{cases} \tag{9}$$

where

$$\mathbf{E}^H_{j,qms}(\mathbf{r}) = \left[\frac{\mathrm{i}m}{Q_j R} H^{(1)}_m(Q_j R)\hat{\mathbf{R}} - H^{(1)\prime}_m(Q_j R)\hat{\boldsymbol{\varphi}}\right] \mathrm{e}^{\mathrm{i}m\varphi}\mathrm{e}^{\mathrm{i}qz}, \tag{10a}$$

$$\mathbf{E}^H_{j,qmp}(\mathbf{r}) = \frac{q}{k_j}\left[\mathrm{i}H^{(1)\prime}_m(Q_j R)\hat{\mathbf{R}} - \frac{m}{Q_j R}H^{(1)}_m(Q_j R)\hat{\boldsymbol{\varphi}} + \frac{Q_j}{q}H^{(1)}_m(Q_j R)\hat{\mathbf{z}}\right] \mathrm{e}^{\mathrm{i}m\varphi}\mathrm{e}^{\mathrm{i}qz}, \tag{10b}$$

are outgoing waves similar to the propagating waves in Eq. (7), but with the Bessel functions J_m substituted by Hankel functions $H^{(1)}_m$, while the reflection and transmission coefficients $r_{m,\sigma\sigma'}$ and $t_{m,\sigma\sigma'}$ are given by (see Supplementary Information)

$$\begin{bmatrix} r_{m,ss} \\ t_{m,ss} \\ r_{m,\mathrm{ps}} \\ t_{m,\mathrm{ps}} \end{bmatrix} = M^{-1} \begin{bmatrix} -\zeta \frac{Q_1}{k_1} H_m^{(1)}(\tilde{Q}_1) \\ -H_m^{(1)\prime}(\tilde{Q}_1) \\ 0 \\ -\zeta \frac{mq}{k_1 \tilde{Q}_1} H_m^{(1)}(\tilde{Q}_1) \end{bmatrix} \quad \text{and}$$

$$\begin{bmatrix} r_{m,sp} \\ t_{m,sp} \\ r_{m,pp} \\ t_{m,pp} \end{bmatrix} = M^{-1} \begin{bmatrix} 0 \\ -\frac{mq}{k_1 \tilde{Q}_1} H_m^{(1)}(\tilde{Q}_1) \\ -\frac{Q_1}{k_1} H_m^{(1)}(\tilde{Q}_1) \\ -\zeta H_m^{(1)\prime}(\tilde{Q}_1) \end{bmatrix}, \tag{11}$$

with the matrix M defined as [40]

$$M = \begin{bmatrix} \frac{\zeta Q_1}{k_1} J_m(\tilde{Q}_1) & \frac{-Q_\mathrm{h}}{k_\mathrm{h}} H_m^{(1)}(\tilde{Q}_\mathrm{h}) & 0 & 0 \\ J_m'(\tilde{Q}_1) & -H_m^{(1)\prime}(\tilde{Q}_\mathrm{h}) & \frac{mq}{k_1 \tilde{Q}_1} J_m(\tilde{Q}_1) & \frac{-mq}{k_\mathrm{h} \tilde{Q}_\mathrm{h}} H_m^{(1)}(\tilde{Q}_\mathrm{h}) \\ 0 & 0 & \frac{Q_1}{k_1} J_m(\tilde{Q}_1) & \frac{-Q_\mathrm{h}}{k_\mathrm{h}} H_m^{(1)}(\tilde{Q}_\mathrm{h}) \\ \frac{\zeta mq}{k_1 \tilde{Q}_1} J_m(\tilde{Q}_1) & \frac{-mq}{k_\mathrm{h} \tilde{Q}_\mathrm{h}} H_m^{(1)}(\tilde{Q}_\mathrm{h}) & \zeta J_m'(\tilde{Q}_1) & -H_m^{(1)\prime}(\tilde{Q}_\mathrm{h}) \end{bmatrix}, \tag{12}$$

in terms of parameters $\tilde{Q}_j = Q_j a$ and $\zeta \equiv \sqrt{\epsilon_1/\epsilon_\mathrm{h}}$. These expressions are obtained by imposing the electromagnetic boundary conditions at $R = a$, specifically the continuity of the $\hat{\boldsymbol{\varphi}}$ and $\hat{\mathbf{z}}$ electric and magnetic field components at the cylinder surface, which automatically guarantees the continuity of the electric displacement and the magnetic field along the $\hat{\mathbf{R}}$ direction. Incidentally, the dispersion relation for cylindrical waveguide modes is obtained from the condition $\det\{M\} = 0$, which signals the existence of a nontrivial solution in the absence of an external field, and leads to the expression

$$\left[\frac{1}{\tilde{Q}_1}\frac{J_m'(\tilde{Q}_1)}{J_m(\tilde{Q}_1)} - \frac{1}{\tilde{Q}_\mathrm{h}}\frac{H_m^{(1)\prime}(\tilde{Q}_\mathrm{h})}{H_m^{(1)}(\tilde{Q}_\mathrm{h})}\right] \times \left[\frac{\epsilon_1}{\tilde{Q}_1}\frac{J_m'(\tilde{Q}_1)}{J_m(\tilde{Q}_1)} - \frac{\epsilon_\mathrm{h}}{\tilde{Q}_\mathrm{h}}\frac{H_m^{(1)\prime}(\tilde{Q}_\mathrm{h})}{H_m^{(1)}(\tilde{Q}_\mathrm{h})}\right] = \left[\frac{mq}{k}\frac{\tilde{Q}_1^2 - \tilde{Q}_\mathrm{h}^2}{(\tilde{Q}_1\tilde{Q}_\mathrm{h})^2}\right]^2 \tag{13}$$

with $k = \omega/c$. The above result is equivalent to other *textbook* forms of the dispersion relation for cylindrical waveguide modes [41–44], typically expressed in terms of modified Bessel functions *in lieu* of Hankel functions. The range of wavelengths λ for which only a single mode exists is determined by the condition $(a/\lambda)\sqrt{\epsilon_1 - \epsilon_\mathrm{h}} < (\alpha_0/2\pi) = 0.3827$, where α_0 is the first zero of J_0, [45] thus setting a wavelength threshold for the multimode waveguide here considered.

4.1.1 Electric field distribution of guided modes: For convenience, we introduce normalized *s*- and *p*-polarized fields defined as

$$\mathbf{E}_i^s(\mathbf{R}) = \begin{cases} \frac{\mathrm{i}k_1}{\sqrt{\epsilon_1}Q_1}\frac{1}{J_m(\tilde{Q}_1)}\mathbf{E}_{1,qms}^J(\mathbf{R}), & R < a, \\ \frac{\mathrm{i}k_\mathrm{h}}{\sqrt{\epsilon_\mathrm{h}}Q_\mathrm{h}}\frac{1}{H_m^{(1)}(\tilde{Q}_\mathrm{h})}\mathbf{E}_{\mathrm{h},qms}^H(\mathbf{R}), & R \geq a, \end{cases} \tag{14a}$$

$$\mathbf{E}_i^p(\mathbf{R}) = \begin{cases} \frac{k_1}{Q_1}\frac{1}{J_m(\tilde{Q}_1)}\mathbf{E}_{1,qmp}^J(\mathbf{R}), & R < a, \\ \frac{k_\mathrm{h}}{Q_\mathrm{h}}\frac{1}{H_m^{(1)}(\tilde{Q}_\mathrm{h})}\mathbf{E}_{\mathrm{h},qmp}^H(\mathbf{R}), & R \geq a, \end{cases} \tag{14b}$$

respectively, such that $\mathbf{E}_i^p \cdot \hat{\mathbf{z}} = 1$ and $\mathbf{H}_i^s \cdot \hat{\mathbf{z}} = 1$, with the magnetic field $\mathbf{H}_i^\sigma = -(\mathrm{i}/k)\nabla \times \mathbf{E}_i^\sigma$ obtained from Faraday's law. Note that without loss of generality we evaluate the modes at $z = 0$, and a global factor $\mathrm{e}^{\mathrm{i}qz}$ is understood to contain the dependence on the coordinate along the waveguide direction z. Guided modes are obtained as solutions of Eq. (13), which for a given *azimuthal* dependence m admits different *radial* solutions (labeled by l), so that the modes are characterized with $\{m, l\}$ indices.

TE and TM modes – For $m = 0$ we see from the secular matrix M in Eq. (12) that s and p components are not mixed by scattering at the circular waveguide surface, and therefore, pure-polarization solutions exist in this case, signaled by the vanishing of one of the two factors in the left-hand side of Eq. (13): TE_{0l} modes (s waves) of electric field $\mathbf{E}_i^s(\mathbf{R})$ (Eq. (14a)) when the first factor is zero; and TM_{0l} modes (p waves) of electric field $\mathbf{E}_i^p(\mathbf{R})$ (Eq. (14b)) when the second factor vanishes.

HE and HE hybrid modes – For $m \neq 0$, the solutions to Eq. (13) are modes of hybrid polarization, EH_{ml} and HE_{ml}, for which both s and p waves contribute, such that the field of mode i can be expressed as $\mathbf{E}_i = \nu \mathbf{E}_i^s + \mathbf{E}_i^p$, where

$$\nu = \frac{\mathrm{i}mq}{k}\frac{\tilde{Q}_1^2 - \tilde{Q}_\mathrm{h}^2}{\tilde{Q}_1\tilde{Q}_\mathrm{h}}\left[\frac{\tilde{Q}_\mathrm{h}J_m'(\tilde{Q}_1)}{J_m(\tilde{Q}_1)} - \frac{\tilde{Q}_1 H_m^{(1)\prime}(\tilde{Q}_\mathrm{h})}{H_m^{(1)}(\tilde{Q}_\mathrm{h})}\right]^{-1}$$

is defined by imposing continuity of the tangential fields at $R = a$. When $\mathrm{i}\nu > 0$ is far from the cutoff frequency, the modes are termed HE_{ml}, while in the opposite situation they are labeled as EH_{ml}. Note that alternative yet equivalent definitions exist depending on how modes are normalized [46].

4.1.2 Waveguided pulses: We consider the propagation of Gaussian wavepackets in the cylindrical waveguide, characterized by a finite spatial pulse width L along the waveguide direction $\hat{\mathbf{z}}$, such that the field is given by

$$\mathbf{E}_i(\mathbf{r}, t) = \int \frac{\mathrm{d}q}{2\pi}\mathbf{E}_i(\mathbf{R}, q)\mathrm{e}^{\mathrm{i}(qz-\omega t)}\left[\sqrt{\pi}L\mathrm{e}^{-(q-q_i)^2L^2/4}\right] + \mathrm{c.c.},$$

where $\mathbf{E}_i(\mathbf{R}, q)$ is the profile of mode i for a wave vector q. In the pulse, q is tightly packed around $q = q_i$. Linearizing the dispersion according to $\omega \approx \omega_i + v_i(q - q_i)$, where $v_i = \partial\omega/\partial q|_{q=q_i}$ is the associated group velocity, and considering L to be large enough to assume that the electric field profile does not vary significantly within a wave vector interval of size $\sim 1/L$ around q_i, such that $\mathbf{E}_i(\mathbf{R}, q) \approx \mathbf{E}_i(\mathbf{R}, q_i) \equiv \mathbf{E}_i(\mathbf{R})$, we can write the field as

$$\mathbf{E}_i(\mathbf{r}, t) \approx \mathbf{E}_i(\mathbf{R})\mathrm{e}^{\mathrm{i}(q_i z - \omega_i t)}\int \frac{\mathrm{d}q}{2\pi}\mathrm{e}^{\mathrm{i}(q-q_i)(z-v_i t)} \times \left[\sqrt{\pi}L\mathrm{e}^{-(q-q_i)^2L^2/4}\right] + \mathrm{c.c.},$$

which, after evaluating the integral in q, reduces to

$$\mathbf{E}_i(\mathbf{r}, t) = \mathbf{E}_i(\mathbf{R})\mathrm{e}^{\mathrm{i}(q_i z - \omega_i t)}\mathrm{e}^{-(z-v_i t)^2/L^2} + \mathrm{c.c.} \tag{15}$$

The corresponding magnetic field is readily computed from Faraday's law $\mathbf{H}_i = -(\mathrm{i}/k)\nabla \times \mathbf{E}_i$ by approximating the ∂_z component of $\nabla = \nabla_\mathbf{R} + \hat{\mathbf{z}}\partial_z$ acting on $\mathbf{E}_i$ as $\mathrm{i}q_i - 2(z - v_i t)/L^2 \approx \mathrm{i}q_i$, provided that the spatial width of the wavepacket L satisfies $q_i L \gg 2\pi$, so that

$$\mathbf{H}_i(\mathbf{r}, t) = \mathbf{H}_i(\mathbf{R})\mathrm{e}^{\mathrm{i}(q_i z - \omega_i t)}\mathrm{e}^{-(z-v_i t)^2/L^2} + \mathrm{c.c.} \tag{16}$$

with $\mathbf{H}_i(\mathbf{R}) = -(\mathrm{i}/k)(\nabla_\mathbf{R} + \mathrm{i}q_i\hat{\mathbf{z}}) \times \mathbf{E}_i(\mathbf{R})$.

4.2 Field produced by an inner line dipole in the region outside the waveguide

We consider a line dipole placed at a transverse position $\mathbf{R}_0 = (x_0, y_0)$ within the waveguide and represent it by a dipole density $\mathbf{p}\,\mathrm{e}^{\mathrm{i}qz_0}$ (dipole per unit length) extending along the line defined by varying z_0 in $(\mathbf{R}_0, z_0)$. It is useful to begin by calculating the electric field produced in a homogeneous medium with the same permittivity ϵ_1 as the waveguide material, expressed as the integral over z_0 of the field due to a point dipole [30]:

$$\mathbf{E}^{\mathrm{dip}}(\mathbf{r}, \mathbf{R}_0) = \frac{1}{\epsilon_1}\left(k_1^2 + \nabla \otimes \nabla\right)\mathbf{p}(\mathbf{R}_0) \int \mathrm{d}z_0\, \frac{\mathrm{e}^{\mathrm{i}k_1|\mathbf{r}-\mathbf{r}_0|}}{|\mathbf{r}-\mathbf{r}_0|}\mathrm{e}^{\mathrm{i}qz_0}, \tag{17}$$

where ∇ is understood to act on $\mathbf{r}$, whereas the integral can be evaluated using the identity $\int \mathrm{d}z_0\, \exp(\mathrm{i}k_1|\mathbf{r}-\mathbf{r}_0| + \mathrm{i}qz_0)/|\mathbf{r}-\mathbf{r}_0| = \mathrm{i}\pi \mathrm{e}^{\mathrm{i}qz} H_0^{(1)}(Q_1|\mathbf{R}-\mathbf{R}_0|)$ with Q_1 defined as in Eq. (7). The line dipole should generate a set of outgoing cylindrical waves (therefore the Hankel functions) centered at $\mathbf{R}_0$, so in order to capitalize on the axial symmetry of the waveguide, we need to express the field in terms of waves centered at the origin $\mathbf{R} = 0$. To this end, we invoke Graf's theorem (see Eq. 9.1.79 in Ref. [47]), $H_0^{(1)}(Q_1|\mathbf{R}-\mathbf{R}_0|) = \sum_m H_m^{(1)}(Q_1 R) J_m(Q_1 R_0)\mathrm{e}^{\mathrm{i}m(\varphi-\varphi_0)}$, which holds for $|\mathbf{R}| > |\mathbf{R}_0|$ and can thus be used to describe the dipole field in the waveguide surface region $R = a > R_0$, through which the outgoing waves are partially transmitted outside the waveguide. This translation formula allows us to recast Eq. (17) into

$$\mathbf{E}^{\mathrm{dip}}(\mathbf{r}, \mathbf{R}_0) = \frac{\mathrm{i}\pi}{\epsilon_1}\sum_m J_m(Q_1 R_0)\mathrm{e}^{-\mathrm{i}m\varphi_0} \times \left[k_1^2 \mathbf{p} + \nabla(\mathbf{p}\cdot\nabla)\right] H_m^{(1)}(Q_1 R)\mathrm{e}^{\mathrm{i}m\varphi}\mathrm{e}^{\mathrm{i}qz}. \tag{18}$$

Now, projecting the dipole as $\mathbf{p} = \sum_\pm p_\pm(\hat{\mathbf{x}} \pm \hat{\mathbf{y}})/\sqrt{2} + p_z\hat{\mathbf{z}}$, where

$$p_\pm = \mathbf{p}\cdot(\hat{\mathbf{x}} \mp \mathrm{i}\hat{\mathbf{y}})/\sqrt{2}, \tag{19a}$$

$$p_z = \mathbf{p}\cdot\hat{\mathbf{z}}, \tag{19b}$$

Eq. (18) can be rewritten as (see Supplementary Information)

$$\mathbf{E}^{\mathrm{dip}}(\mathbf{R}, \mathbf{R}_0) = \pi k^2 \sum_m J_m(k_1 R_0)\mathrm{e}^{-\mathrm{i}m\varphi_0} \times \left[\sum_\pm \frac{p_\pm}{\sqrt{2}}\left(\mathbf{E}^H_{1,q(m\pm1)s} \pm \frac{q}{k_1}\mathbf{E}^H_{1,q(m\pm1)p}\right) + \mathrm{i}p_z\frac{Q_1}{k_1}\mathbf{E}^H_{1,qmp}\right],$$

where the fields $\mathbf{E}^H_{1,qm\sigma}(\mathbf{R})$ are defined in Eq. (7).

4.2.1 Normal emission into the far field: The transmission of electromagnetic fields from the waveguide is determined from Eqs. (9) and (11), which show that, for the special case of $q = 0$ considered here, polarization states do not mix (i.e., $t_{m,\sigma\sigma'} = 0$ for $\sigma \neq \sigma'$). We thus express the field outside the waveguide produced by a line dipole $\mathbf{p}$ placed at $\mathbf{R}_0$ as

$$\mathbf{E}^{\mathrm{out}}(\mathbf{R}, \mathbf{R}_0) = \pi k^2 \sum_m J_m(k_1 R_0)\mathrm{e}^{-\mathrm{i}m\varphi_0} \times \left[\frac{p_+}{\sqrt{2}} t_{m+1,ss}\mathbf{E}^H_{\mathrm{h},0(m+1)s} + \frac{p_-}{\sqrt{2}} t_{m-1,ss}\mathbf{E}^H_{\mathrm{h},0(m-1)s} + \mathrm{i}p_z t_{m,pp}\mathbf{E}^H_{\mathrm{h},0mp}\right], \tag{20}$$

which is obviously independent of z. In the far field, we can use the asymptotic limit $H_m^{(1)}(\theta) \approx \sqrt{2/\pi\theta}\,\mathrm{e}^{\mathrm{i}(\theta - m\pi/2 - \pi/4)}$ (see Eq. 10.17.5 in Ref. [48]) for large arguments of the Hankel functions in the outgoing waves $\mathbf{E}^H_{j,0m\sigma}$ (see Eq. (10)), which allows us to write the electric field as

$$\mathbf{E}^H_{\mathrm{h},0m\sigma}(\mathbf{R}) \underset{k_\mathrm{h}R\gg1}{\to} \frac{\mathrm{e}^{\mathrm{i}k_\mathrm{h}R}}{\sqrt{k_\mathrm{h}R}}\sqrt{\frac{2}{\pi}}\,\mathrm{e}^{\mathrm{i}(m\varphi - m\pi/2 - \pi/4)} \begin{cases} -\mathrm{i}\hat{\boldsymbol{\varphi}}, & (\sigma = s), \\ \hat{\mathbf{z}}, & (\sigma = p), \end{cases}$$

while the magnetic far field is obtained by using Eq. (8) and Faraday's law as $\mathbf{H}^H_{\mathrm{h},0m\sigma} \xrightarrow[k_\mathrm{h}R\gg1]{} -\mathrm{i}\sqrt{\epsilon_\mathrm{h}}\,\mathbf{E}^H_{\mathrm{h},0m\sigma'}$ with $\sigma' \neq \sigma$. Applying these expressions to Eq. (20), we find the far electric field

$$\mathbf{E}^{\mathrm{out}}(\mathbf{R}, \mathbf{R}_0) \xrightarrow[k_\mathrm{h}R\gg1]{} \left[\mathcal{S}^+(\hat{\mathbf{R}}, \mathbf{R}_0, q, \omega)p_+ + \mathcal{S}^-(\hat{\mathbf{R}}, \mathbf{R}_0, q, \omega)p_- + \mathcal{S}^z(\hat{\mathbf{R}}, \mathbf{R}_0, q, \omega)p_z\right]\frac{\mathrm{e}^{\mathrm{i}k_\mathrm{h}R}}{\sqrt{k_\mathrm{h}R}}, \tag{21}$$

where

$$\mathcal{S}^\pm(\hat{\mathbf{R}}, \mathbf{R}_0, \omega) = \pm\mathrm{e}^{3\mathrm{i}\pi/4}\sqrt{\pi}k^2\,\hat{\boldsymbol{\varphi}}\sum_m \mathrm{i}^{-m}J_m(k_1 R_0) \times \mathrm{e}^{\mathrm{i}[(m\pm1)\varphi - m\varphi_0]}\,t_{m\pm1,ss}, \tag{22a}$$

$$\mathcal{S}^z(\hat{\mathbf{R}}, \mathbf{R}_0, \omega) = \mathrm{e}^{\mathrm{i}\pi/4}\sqrt{2\pi}k^2\,\hat{\mathbf{z}}\sum_m \mathrm{i}^{-m}J_m(k_1 R_0) \times \mathrm{e}^{\mathrm{i}m(\varphi-\varphi_0)}\,t_{m,pp}, \tag{22b}$$

and the dipole components are defined in Eq. (19).

The above relations allow us to obtain explicit expressions for the far-field limit ($k_\mathrm{h}R \gg 1$) of the two-dimensional electromagnetic Green tensor $\mathcal{G}_{2\mathrm{D}}(\mathbf{R}, \mathbf{R}_0, \omega)$, which is implicitly defined through the expression $\mathbf{E}^{\mathrm{out}}(\mathbf{R}, \mathbf{R}_0) = \mathcal{G}_{2\mathrm{D}}(\mathbf{R}, \mathbf{R}_0, \omega)\cdot\mathbf{p}$, relating the strength $\mathbf{p}$ of a uniform line dipole placed at $\mathbf{R}_0$ inside the waveguide to the electric field $\mathbf{E}^{\mathrm{out}}(\mathbf{R}, \mathbf{R}_0)$ that it generates at a position $\mathbf{R}$ outside it. Taking into consideration the general asymptotic relation $\mathcal{G}_{2\mathrm{D}}(\mathbf{R}, \mathbf{R}_0, \omega) \xrightarrow[k_\mathrm{h}R\gg1]{} \left(\mathrm{e}^{\mathrm{i}k_\mathrm{h}R}/\sqrt{k_\mathrm{h}R}\right)\mathbf{S}(\hat{\mathbf{R}}, \mathbf{R}_0, \omega)$, and comparing it to Eqs. (21) and (22), we can readily write $\mathcal{S}^\pm = \mathbf{S}\cdot(\hat{\mathbf{x}} \pm \mathrm{i}\hat{\mathbf{y}})/\sqrt{2}$ and $\mathcal{S}^z = \mathbf{S}\cdot\hat{\mathbf{z}}$ to obtain the explicit formula in Eq. (34). These results can be easily generalized to off-normal emission ($q \neq 0$), but involve off-diagonal transmission coefficients that lead to more complicated expressions.

4.3 Sum-frequency generation by counter-propagating waveguided pulses

We now introduce counter-propagating pulse fields $\mathbf{E}_i(\mathbf{r}, t)$ and $\mathbf{E}_{i'}(\mathbf{r}, t)$ of the form given in Eq. (15), oscillating at frequencies ω_i and $\omega_{i'}$,

respectively. Through the second-order nonlinearity of the waveguide material $\chi^{(2)}_{abc}$, where the subscripts a, b, and c denote Cartesian components, a polarization density $\mathbf{P}_{ii'}$ is produced at frequency $\omega_{ii'} = \omega_i + \omega_{i'}$. More precisely,

$$\mathbf{P}_{ii'}(\mathbf{r},t) = |\bar{\chi}^{(2)}|\tilde{\mathbf{P}}_{ii'}(\mathbf{r},t), \tag{23}$$

where $|\bar{\chi}^{(2)}|$, defined in Eq. (3), is introduced to quantify the strength of the SF susceptibility, while the normalized polarization density can be separated as

$$\tilde{\mathbf{P}}_{ii'}(\mathbf{r},t) = \tilde{\mathbf{P}}_{ii'}(\mathbf{R})\, S_{ii'}(z,t) + \text{c.c.} \tag{24}$$

by defining $\tilde{\mathbf{P}}_{ii'}(\mathbf{R})$ as in Eq. (2), as well as the (z,t)-dependent factor

$$S_{ii'}(z,t) = \mathrm{e}^{\mathrm{i}[(q_i+q_{i'})z-\omega_{ii'}t]}\mathrm{e}^{-(z-v_i t)^2/L^2}\mathrm{e}^{-(z-v_{i'}t)^2/L^2}. \tag{25}$$

Eventually, we set $q_i = -q_{i'}$ (i.e., waveguided photons with opposite wave vectors, leading to normal emission of SF photons), so v_i and $v_{i'}$ also have opposite signs inherited from q_i and $q_{i'}$. In addition, the nonlinear susceptibility $\chi^{(2)}_{abc}(\mathbf{r})$ is taken to be constant over the range of frequencies under consideration, as well as uniform inside the waveguide and zero outside it. We note that the present analysis could be trivially extended to consider a nonlinear cladding instead.

The SF field $\mathbf{E}_{ii'}(\mathbf{r},t)$ is thus produced by the nonlinear polarization density according to

$$\begin{aligned}\mathbf{E}_{ii'}(\mathbf{r},t) &= \int \frac{\mathrm{d}\omega}{2\pi}\mathrm{e}^{-\mathrm{i}\omega t}\,\mathbf{E}_{ii'}(\mathbf{r},\omega)\\ &= \int \frac{\mathrm{d}\omega}{2\pi}\mathrm{e}^{-\mathrm{i}\omega t}\int \mathrm{d}^3\mathbf{r}'\,\mathcal{G}(\mathbf{r},\mathbf{r}',\omega)\cdot\int \mathrm{d}t'\mathrm{e}^{\mathrm{i}\omega t'}\mathbf{P}_{ii'}(\mathbf{r}',t'),\end{aligned} \tag{26}$$

where we have introduced the three-dimensional electromagnetic Green tensor $\mathcal{G}(\mathbf{r},\mathbf{r}',\omega)$, defined in such a way that $\mathbf{E}(\mathbf{r},\mathbf{r}') = \mathcal{G}(\mathbf{r},\mathbf{r}',\omega)\cdot\mathbf{p}$ gives the field produced at $\mathbf{r}$ by a point dipole of strength $\mathbf{p}$ placed at $\mathbf{r}'$. To quantify SF generation in the far-field limit (i.e., at $k_{\mathrm{h}}r \gg 1$), we exploit the translational invariance of the polarization source to write

$$\begin{aligned}\mathcal{G}(\mathbf{r},\mathbf{r}',\omega) = \mathcal{G}(\mathbf{r}-z'\hat{\mathbf{z}},\mathbf{R}',\omega) &\underset{k_{\mathrm{h}}r\gg1}{\to}\\ \frac{\mathrm{e}^{\mathrm{i}k_{\mathrm{h}}r}}{r}\mathrm{e}^{-\mathrm{i}k_{\mathrm{h}}zz'/r}&\mathbf{g}(\hat{\mathbf{r}},\mathbf{R}',\omega),\end{aligned} \tag{27}$$

which allows us to recast Eq. (26) as

$$\mathbf{E}_{ii'}(\mathbf{r},t) = \int \frac{\mathrm{d}\omega}{2\pi}\mathrm{e}^{-\mathrm{i}\omega t}\frac{\mathrm{e}^{\mathrm{i}k_{\mathrm{h}}r}}{r}\mathbf{f}_{ii'}(\hat{\mathbf{r}},\omega) \tag{28}$$

in terms of the frequency-space electric far-field amplitude

$$\begin{aligned}\mathbf{f}_{ii'}(\hat{\mathbf{r}},\omega) = &\int \mathrm{d}^3\mathbf{r}'\,\mathrm{e}^{-\mathrm{i}k_{\mathrm{h}}zz'/r}\\ &\times\mathbf{g}(\hat{\mathbf{r}},\mathbf{R}',\omega)\cdot\int \mathrm{d}t'\mathrm{e}^{\mathrm{i}\omega t'}\mathbf{P}_{ii'}(\mathbf{r}',t').\end{aligned} \tag{29}$$

Finally, as shown in Supplementary Information, we can relate the far-field three-dimensional amplitude obtained from the Green tensor in Eqs. (27) and (29) to the two-dimensional one presented in Section (4.2.1) as

$$\mathbf{g}^j(\hat{\mathbf{r}},\mathbf{R}',\omega) = \frac{\mathrm{e}^{-\mathrm{i}\pi/4}}{\sqrt{2\pi}}\mathcal{S}^j(\hat{\mathbf{R}},\mathbf{R}',q,\omega),$$

with j taking the values $+$, $-$, and z. Again, explicit expressions for the components of $\mathbf{S}(\hat{\mathbf{R}},\mathbf{R}',q,\omega)$ are offered in Section 4.2.1.

4.4 Up- and down-conversion efficiency

The efficiency of the SPDC process in which a photon impinging normally to the waveguide direction produces a pair of guided photons moving in opposite directions away from one another is argued to be identical with that of an up-conversion process involving SF generation of two guided photons moving toward one another, provided that reciprocity applies. We then calculate the SF efficiency $\eta_{ii'} = N_{ii'}/N_i N_{i'}$ as the ratio of the number of emitted SF photons $N_{ii'}$ to the number of incident photons N_i and $N_{i'}$ in both guided pulses.

The number of photons carried by a guided mode pulse with field profile $\mathbf{E}_i(\mathbf{r},t)$ is expressed as

$$N_i = \frac{1}{\hbar\omega_i}\int_{-\infty}^{\infty}\mathrm{d}t\int \mathrm{d}^2\mathbf{R}\;\mathbf{S}_i(\mathbf{r},t)\cdot\hat{\mathbf{z}},$$

where we evaluate the flux carried by the Poynting vector $\mathbf{S}_i(\mathbf{r},t) = (c/4\pi)\mathbf{E}_i(\mathbf{r},t)\times\mathbf{H}_i(\mathbf{r},t)$ in the $\mathbf{R}$ plane. Inserting the fields given by Eqs. (15) and (16) and integrating over time, we obtain

$$N_i = \frac{cL}{2\sqrt{2\pi}|v_i|}\frac{1}{\hbar\omega_i}\int d^2\mathbf{R}\;\mathrm{Re}\left\{E_{i,x}H^*_{i,y} - E_{i,y}H^*_{i,x}\right\}. \tag{30}$$

Likewise, the number of photons produced in the far field via SF generation from the radial component of the energy emanating from the waveguide can be in turn obtained from the far-field Poynting vector $\mathbf{S}^{\infty}_{ii'}$ (evaluated from the field in Eq. (28)) as

$$\begin{aligned}N_{ii'} &= \frac{1}{\hbar\omega_{ii'}}\int_{-\infty}^{\infty}\mathrm{d}t\int \mathrm{d}\Omega_{\hat{\mathbf{r}}}\,r^2\,\hat{\mathbf{R}}\cdot\mathbf{S}^{\infty}_{ii'}(\mathbf{r},t)\\ &= \frac{\sqrt{\epsilon_{\mathrm{h}}}c}{4\pi^2\hbar\omega_{ii'}}\int \mathrm{d}\Omega_{\hat{\mathbf{r}}}\,(\hat{\mathbf{R}}\cdot\hat{\mathbf{r}})\int_0^{\infty}\mathrm{d}\omega\left|\mathbf{f}_{ii'}(\hat{\mathbf{r}},\omega)\right|^2.\end{aligned} \tag{31}$$

In the derivation of the above expression, we have used the fact that $\mathbf{f}_{ii'}(\hat{\mathbf{r}},\omega)\cdot\hat{\mathbf{r}} = 0$ (i.e., the far field is transverse). For long pulses (see Eq. (15)), only the first term in Eq. (24) (peaked around frequencies $\omega\sim\omega_{ii'}$) contributes to $\mathbf{f}_{ii'}(\hat{\mathbf{r}},\omega)$ over the $\omega>0$ integral in Eq. (31), and therefore, using Eqs. (23), (24), and (29), we can write

$$\begin{aligned}\int_0^{\infty}\mathrm{d}\omega\left|\mathbf{f}_{ii'}(\hat{\mathbf{r}},\omega)\right|^2 \approx 2\pi|\bar{\chi}^{(2)}|^2 A_{ii'}&\\ \times\left|\int_{R'<a}\mathrm{d}^2\mathbf{R}'\,\mathbf{g}\left(\hat{\mathbf{r}},\mathbf{R}',\omega_{ii'}\right)\cdot\tilde{\mathbf{P}}_{ii'}(\mathbf{R}')\right|^2&.\end{aligned}$$

where

$$\begin{aligned}A_{ii'} &= \frac{1}{2\pi}\int_0^{\infty}\mathrm{d}\omega\left|\int\mathrm{d}z'\int\mathrm{d}t\,\mathrm{e}^{-\mathrm{i}k_{\mathrm{h}}zz'/r}\,\mathrm{e}^{\mathrm{i}\omega t}\,S_{ii'}(z',t)\right|^2\\ &\approx \frac{1}{2\pi}\int_{-\infty}^{\infty}\mathrm{d}\omega\left|\int\mathrm{d}z'\int\mathrm{d}t\,\mathrm{e}^{-\mathrm{i}k_{\mathrm{h}}zz'/r}\,\mathrm{e}^{\mathrm{i}\omega t}\,S_{ii'}(z',t)\right|^2\\ &= \int\mathrm{d}t\left|\int\mathrm{d}z'\,\mathrm{e}^{-\mathrm{i}k_{\mathrm{h}}zz'/r}\,S_{ii'}(z',t)\right|^2,\\ &= \frac{\pi^{3/2}L^3}{2|v_i-v_{i'}|}\mathrm{e}^{-(q_i+q_{i'}-q)^2L^2/4}\end{aligned}$$

with $q = \left(\sqrt{\epsilon_\mathrm{h}}\omega_{ii'}/c\right) z/r$. Here, we have approximated ω by $\omega_{ii'}$ in $\mathbf{g}(\hat{\mathbf{r}}, \mathbf{R}', \omega)$ and k_h (because the incident pulses are long enough to be considered narrowly peaked around their respective central frequencies ω_i and $\omega_{i'}$), extended the ω range of integration to nonresonant negative values, used Plancharel's theorem, and taken $S_{ii'}(z', t)$ from Eq. (25) to analytically evaluate the remaining integrals. In addition, we can carry out the polar-angle integral in Eq. (31) by writing $\mathrm{d}\Omega_{\hat{\mathbf{r}}} = \mathrm{d}\varphi \mathrm{d}q \times \left(c/\sqrt{\epsilon_\mathrm{h}}\omega_{ii'}\right)$ and considering that the pulse length L is sufficiently large as to make $A_{ii'}$ negligible outside the light cone $|q| < \sqrt{\epsilon_\mathrm{h}}\omega_{ii'}/c$. This leads to

$$N_{ii'} = \int_0^{2\pi} \mathrm{d}\varphi N_{ii'}(\varphi) \tag{32}$$

with

$$N_{ii'}(\varphi) = |\vec{\chi}^{(2)}|^2 \frac{\pi L^2 c^2}{2\hbar\omega_{ii'}^2 |v_i - v_{i'}|} (\hat{\mathbf{R}} \cdot \hat{\mathbf{r}}) \times \left| \int_{R'<a} \mathrm{d}^2\mathbf{R}' \, \mathbf{g}\left(\hat{\mathbf{r}}, \mathbf{R}', \omega_{ii'}\right) \cdot \tilde{\mathbf{P}}_{ii'}(\mathbf{R}') \right|^2, \tag{33}$$

where the direction $\hat{\mathbf{r}}$ is defined by the azimuthal angle φ and the component $q_i + q_{i'}$ of the emitted light wave vector along the axis of the cylindrical waveguide.

Finally, we specialize the above expressions to $q_i + q_{i'} = 0$ (normal emission, for which $\hat{\mathbf{R}} \cdot \hat{\mathbf{r}} = 1$) and evaluate the efficiency $\eta_{ii'} = N_{ii'}/N_i N_{i'}$ by using Eqs. (30), (32), and (33), from which we find the result shown in Eqs. (4) and (5), where we have explicitly indicated the dependence of the far-field Green tensor

$$\mathbf{g}(\hat{\mathbf{r}}, \mathbf{R}', \omega) = \mathbf{g}(\varphi - \varphi', R', \omega) = k^2 \sum_m \mathrm{i}^{-m} J_m\left(k_1 R'\right) \times \mathrm{e}^{\mathrm{i}m(\varphi-\varphi')} \left[t_{m,pp} \, \hat{\boldsymbol{\varphi}} \otimes \hat{\boldsymbol{\varphi}} + \frac{1}{2} \sum_{\pm} \mathrm{t}_{\mathrm{m}\pm1,\mathrm{ss}} \, \hat{\boldsymbol{\varphi}} \otimes (\hat{\boldsymbol{\varphi}} \pm \mathrm{i}\hat{\mathbf{R}}) \right] \tag{34}$$

on the difference of the azimuthal angles of $\hat{\mathbf{r}}$ and $\mathbf{R}'$ in the $\{\hat{\mathbf{R}}, \hat{\varphi}, \hat{\mathbf{z}}\}$ frame (see Supplementary Information).

Author contribution: All the authors have accepted responsivity for the entire content of this manuscript and approved.

Research funding: This work has been supported in part by ERC (Advanced Grant 789 104-eNANO), the Spanish MICINN (PID2020-112625GB-I00 and SEV2015-0522), the Catalan CERCA Program, the Generalitat de Catalunya, the European Social Fund (L'FSE inverteix en el teu futur)-FEDER. J. D. C. is a Sapere Aude research leader supported by Independent Research Fund Denmark (grant no. 0165-00051B). The Center for Nano Optics is financially supported by the University of Southern Denmark (SDU 2020 funding).

Conflict of interest statement: The author declares no conflicts of interest regarding this article.

References

[1] S.-B. Zheng and G.-C. Guo, "Efficient scheme for two-atom entanglement and quantum information processing in cavity QED," *Phys. Rev. Lett.*, vol. 85, p. 2392, 2000.

[2] J. M. Raimond, M. Brune, and S. Haroche, "Manipulating quantum entanglement with atoms and photons in a cavity," *Rev. Mod. Phys.*, vol. 73, p. 565, 2001.

[3] A. Lamas-Linares, J. C. Howell, and D. Bouwmeester, "Stimulated emission of polarization-entangled photons," *Nature*, vol. 412, p. 887, 2001.

[4] C. Monroe, "Quantum information processing with atoms and photons," *Nature*, vol. 416, p. 238, 2002.

[5] T. Inagaki, N. Matsuda, O. Tadanaga, M. Asobe, and H. Takesue, "Entanglement distribution over 300 km of fiber," *Opt. Express*, vol. 21, p. 23241, 2013.

[6] S.-K. Liao, W.-Q. Cai, W.-Y. Liu, et al., "Satellite-to-ground quantum key distribution," *Nature*, vol. 549, p. 43, 2017.

[7] D. E. Chang, V. Vuletić, and M. D. Lukin, "Quantum nonlinear optics - photon by photon," *Nat. Photon.*, vol. 8, p. 685, 2014.

[8] X. Li, P. L Voss, J. E. Sharping, and P. Kumar, "Optical-fiber source of polarization-Entangled photons in the 1550 nm telecom band," *Phys. Rev. Lett.*, vol. 94, 2005, Art no. 053601.

[9] J. Liu, I. Nape, Q. Wang, A. Vallés, J. Wang, and A. Forbes, "Multidimensional entanglement transport through single-mode fiber," *Sci. Adv.*, vol. 6, 2020, Art no. eaay0837.

[10] A. Mair, A. Vaziri, G. Weihs, and A. Zeilinger, "Entanglement of the orbital angular momentum states of photons," *Nature*, vol. 412, p. 313, 2001.

[11] R. Fickler, R. Lapkiewicz, W. N. Plick, et al., "Quantum entanglement of high angular momenta," *Science*, vol. 338, p. 640, 2012.

[12] M. Malik, M. Erhard, M. Huber, M. Krenn, R. Fickler, and A. Zeilinger, "Multi-photon entanglement in high dimensions," *Nat. Photon.*, vol. 10, p. 248, 2016.

[13] T. Stav, A. Faerman, E. Maguid, et al., "Quantum entanglement of the spin and orbital angular momentum of photons using metamaterials," *Science*, vol. 361, p. 1101, 2018.

[14] A. S. Solntsev, G. S. Agarwal, and Y. S. Kivshar, "Metasurfaces for quantum photonics," *Nat. Photon.*, vol. 15, p. 327, 2021.

[15] P. G. Kwiat, K. Mattle, H. Weinfurter, A. Zeilinger, A. V. Sergienko, and Y. Shih, "New high-intensity source of polarization-entangled photon pairs," *Phys. Rev. Lett.*, vol. 75, p. 4337, 1995.

[16] H. H. Arnaut and G. A. Barbosa, "Orbital and intrinsic angular momentum of single photons and entangled pairs of photons generated by parametric down-conversion," *Phys. Rev. Lett.*, vol. 85, p. 286, 2000.

[17] R. W. Boyd, *Nonlinear Optics*, 3rd ed. Amsterdam, Academic, 2008.

[18] L. G. Helt and M. J. Steel, "Effect of scattering loss on connections between classical and quantum processes in second-order nonlinear waveguides," *Opt. Lett.*, vol. 40, p. 1460, 2015.

[19] R. van der Meer, J. J. Renema, B. Brecht, C. Silberhorn, and P. W. Pinkse, "Optimizing spontaneous parametric down-conversion sources for boson sampling," *Phys. Rev. A*, vol. 101, 2020, Art no. 063821.

[20] Z. Yang, M. Liscidini, and J. E. Sipe, "Spontaneous parametric down-conversion in waveguides: a backward Heisenberg picture approach," *Phys. Rev. A*, vol. 77, 2008, Art no. 033808.
[21] L. G. Helt, M. J. Steel, and J. E. Sipe, "Spontaneous parametric downconversion in waveguides: what's loss got to do with it?," *New J. Phys.*, vol. 17, 2015, Art no. 013055.
[22] F. Lenzini, A. N. Poddubny, J. Titchener, et al., "Direct characterization of a nonlinear photonic circuit's wave function with laser light," *Light Sci. Appl.*, vol. 7, p. 17143, 2018.
[23] E. Pomarico, B. Sanguinetti, N. Gisin, et al., "Waveguide-based OPO source of entangled photon pairs," *New J. Phys.*, vol. 11, p. 113042, 2009.
[24] K.-H. Luo, H. Herrmann, S. Krapick, et al., "Direct generation of genuine single-longitudinal-mode narrowband photon pairs," *New J. Phys.*, vol. 17, 2015, Art no. 073039.
[25] V. S. Ilchenko, A. A. Savchenkov, A. B. Matsko, and L. Maleki, "Nonlinear optics and crystalline whispering gallery mode cavities," *Phys. Rev. Lett.*, vol. 92, 2004, Art no. 043903.
[26] X. Guo, C.-l. Zou, C. Schuck, H. Jung, R. Cheng, and H. X. Tang, "Parametric down-conversion photon-pair source on a nanophotonic chip," *Light Sci. Appl.*, vol. 6, 2017, Art no. e16249.
[27] J. W. Silverstone, D. Bonneau, K. Ohira, et al., "On-chip quantum interference between silicon photon-pair sources," *Nat. Photon.*, vol. 8, p. 104, 2014.
[28] F. Setzpfandt, A. S. Solntsev, J. Titchener, et al., "Tunable generation of entangled photons in a nonlinear directional coupler," *Laser Photon. Rev.*, vol. 10, p. 131, 2016.
[29] Z. Sun, D. Basov, and M. Fogler, "Graphene as a source of entangled plasmons," arXiv preprint arXiv:2110.14917, 2021.
[30] L. Novotny and B. Hecht, *Principles of Nano-Optics*, Cambridge, Cambridge University Press, 2006.
[31] A. De Rossi and V. Berger, "Counterpropagating twin photons by parametric fluorescence," *Phys. Rev. Lett.*, vol. 88, 2002, Art no. 043901.
[32] M. C. Booth, M. Atatüre, G. Di Giuseppe, B. E. Saleh, A. V. Sergienko, and M. C. Teich, "Counterpropagating entangled photons from a waveguide with periodic nonlinearity," *Phys. Rev. A*, vol. 66, 2002, Art no. 023815.
[33] A. Orieux, X. Caillet, A. Lemaître, P. Filloux, I. Favero, G. Leo, and S. Ducci, "Efficient parametric generation of counterpropagating two-photon states," *J. Opt. Soc. Am. B*, vol. 28, p. 45, 2011.
[34] A. Orieux, A. Eckstein, A. Lemaître, et al., "Direct Bell states generation on a III-V semiconductor chip at room temperature," *Phys. Rev. Lett.*, vol. 110, p. 160502, 2013.
[35] S. Saravi, T. Pertsch, and F. Setzpfandt, "Generation of counterpropagating path-entangled photon pairs in a single periodic waveguide," *Phys. Rev. Lett.*, vol. 118, p. 183603, 2017.
[36] M. B. Plenio and S. S. Virmani, *An Introduction to Entanglement Theory*, Cham, Springer International Publishing, 2014, pp. 173–209.
[37] H. Jin, F. M. Liu, P. Xu, et al., "On-chip generation and manipulation of entangled photons based on reconfigurable lithium-niobate waveguide circuits," *Phys. Rev. Lett.*, vol. 113, p. 103601, 2014.
[38] Y. Kong, F. Bo, W. Wang, D. Zheng, H. Liu, G. Zhang, R. Rupp, and J. Xu, "Recent progress in lithium niobate: optical damage, defect simulation, and on-chip devices," *Adv. Mater.*, vol. 32, p. 1806452, 2020.
[39] V. G. Dmitriev, G. G. Gurzadyan, and D. N. Nikogosyan, *Handbook of Nonlinear Optical Crystals*, vol. 64, 3rd ed. Berlin, Springer, 1999.
[40] F. J. García de Abajo, A. Rivacoba, N. Zabala, and P. M. Echenique, "Electron energy loss spectroscopy as a probe of two-dimensional photonic crystals," *Phys. Rev. B*, vol. 68, p. 205105, 2003.
[41] G. P. Agrawal, *Nonlinear Science at the Dawn of the 21st Century*, Berlin, Springer, 2000.
[42] G. Keiser, *Optical Fiber Communications*, New York, McGraw-Hill, 2011.
[43] D. Marcuse, *Theory of Dielectric Optical Waveguides*, 2nd ed. San Diego, Academic Press, 2013.
[44] R. Engelbrecht, *Nichtlineare Faseroptik: Grundlagen Und Anwendungsbeispiele*, Berlin, Springer-Verlag, 2015.
[45] B. E. Saleh and M. C. Teich, *Fundamentals of Photonics*, New York, John Wiley & Sons, 2019.
[46] C. Yeh and F. I. Shimabukuro, *The Essence of Dielectric Waveguides*, Berlin, Springer, 2008.
[47] M. Abramowitz and I. A. Stegun, *Handbook of Mathematical Functions*, New York, Dover, 1972.
[48] DLMF, *NIST Digital Library of Mathematical Functions*, Release 1.1.3 of 2021-09-15, f. W. J Olver, A. B. Olde Daalhuis, D. W. Lozier, et al., Eds. Available at: http://dlmf.nist.gov/.

Supplementary Material: The online version of this article offers supplementary material (https://doi.org/10.1515/nanoph-2021-0736).